
Impact of the winter North-Atlantic weather regimes on subtropical sea-surface height variability

Nicolas Barrier^{1,*}, Anne-Marie Treguier¹, Christophe Cassou², Julie Deshayes¹

¹ Laboratoire de Physique des océans, CNRS-Ifremer-UBO-IRD, UMR 6523, Brest, France

² CNRS Cerfacs, Toulouse, France

*: Corresponding author : Nicolas Barrier, email address : Nicolas.Barrier@ifremer.fr

Abstract:

Interannual variability of subtropical sea-surface-height (SSH) anomalies, estimated by satellite and tide-gauge data, is investigated in relation to wintertime daily North-Atlantic weather regimes. Sea-level anomalies can be viewed as proxies for the subtropical gyre intensity because of the intrinsic baroclinic structure of the circulation. Our results show that the strongest correlation between SSH and weather regimes is found with the so-called Atlantic-Ridge (AR) while no significant values are obtained for the other regimes, including those related to the North Atlantic Oscillation (NAO), known as the primary actor of the Atlantic dynamics. Wintertime AR events are characterized by anticyclonic wind anomalies off Europe leading to a northward shift of the climatological wind-stress curl. The latter affects subtropical SSH annual variability by altered Sverdrup balance and ocean Rossby wave dynamics propagating westward from the African coast towards the Caribbean. The use of a simple linear planetary geostrophic model allows to quantify those effects and confirms the primary importance of the winter season to explain the largest part of SSH interannual variability in the Atlantic subtropical gyre. Our results open new perspectives in the comprehension of North-Atlantic Ocean variability emphasizing the role of AR as a driver of interannual variability at least of comparable importance to NAO.

1 Introduction

In the context of climate change, the detection of multi-decadal trends and their potential attribution to human influence is a major challenge. A special attention is devoted to sea-surface height (SSH) that integrates the forcings, whatever their origins (natural such as volcanic/tropospheric aerosols and solar fluctuations, or anthropogenic such as sulfates and greenhouse gases emission, etc.), over long periods of time. Its recent accelerating rise is expected to have regionally potential disastrous impacts. Observed SSH variability from seasonal to decadal timescales can be considered as a superimposition of a global upward trend in response to external forcings and a signal associated with intrinsic or natural variability of the climate system. The latter is due to the coupling between components of very different time-scale and spatial-scale characteristics of variability and to the presence of nonlinear processes. Its variance is presently one order of magnitude larger than the externally-forced component and it is thus necessary to quantify and understand the mechanisms of that natural variability to be able to remove it from the observed records and assess long-term trends. In the North-Atlantic, ocean

41 variability mostly comes from changes in wind and buoyancy forcings related to
42 large-scale modes of atmospheric variability. From daily to decadal timescales,
43 the North-Atlantic Oscillation (NAO) is the dominant pattern in the Northern
44 Atlantic/Europe domain. As a matter of fact, many studies were devoted to inves-
45 tigate the impacts of NAO on ocean circulation, especially on SSH and meridional
46 heat transport (MHT) anomalies. MHT anomalies influence basin-scale SSH in
47 turn, via heat content changes (Hakkinen 1999; Esselborn and Eden 2001). We
48 briefly review, below, a selection that is relevant for our study.

49 Ezer (1999) used sensitivity experiments of an ocean model to surface forc-
50 ing to investigate the variability of the subtropical gyre. His results suggest that
51 changes in wind-patterns in the northeastern Atlantic, that he attributes to NAO,
52 cause negative surface elevation. The proposed mechanism is the westward propa-
53 gation of long Rossby waves, consistently with Cabanes et al (2006) and references
54 therein. Hakkinen (1999) argues from a forced ocean model that the NAO is the
55 dominant forcing of MHT via altered surface forcings (wind-stress and heat fluxes).
56 The author states that MHT immediate response to changes in NAO occurs via
57 anomalous Ekman transport, while the low-frequency response mainly occurs via
58 the integration of NAO-induced heat fluxes in the subpolar gyre and the south-
59 ward export of Labrador Sea Water, that causes MHT anomalies to propagate
60 from 45°N to 25°N within one year. Both Eden and Willebrand (2001) and Gulev
61 et al (2003) show an immediate MHT response likely driven by NAO-related wind
62 anomalies. However, their numerical experiments show a delayed ocean response
63 of different nature. While in Eden and Willebrand (2001) the lagged baroclinic re-
64 sponse is mainly wind-driven, Gulev et al (2003) argue that it is due to buoyancy
65 forcing and Labrador Sea Water formation in the subpolar gyre. Esselborn and

66 Eden (2001) investigate, from satellite data and forced ocean model, basin-scale
67 SSH interannual variability in relation with the NAO. They argue that the im-
68 mediate response to a switch from a positive to a negative NAO phase induces a
69 dipole pattern, with negative anomalies in the subpolar gyre and positive anoma-
70 lies in the subtropical gyre. They propose that NAO-related changes in wind-
71 stress curl leads to ocean circulation anomalies that induces anomalous advection
72 of temperature (term $\overline{u'T}$). This leads to anomalous heat convergence/divergence
73 that in turn induces this SSH dipole pattern. The impacts of NAO on subpolar
74 and subtropical gyres have also been investigated from observations. Curry and
75 McCartney (2001) use observed potential energy anomalies (PEA), that can be
76 reflected in SSH anomalies, to estimate the impact of NAO on both gyres. They
77 argue that NAO-induced PEA in the subtropical gyre are dominated by vertical
78 displacements of the pycnocline, driven by open-ocean wind-stress forcing inte-
79 grated westward (see also Sturges and Hong 1995; Sturges et al 1998; Hong et al
80 2000). But changes in the Eighteen Degree Water property (Joyce et al 2000) and
81 changes in the deep ocean (due to altered import of Labrador Sea Water, Curry
82 et al 1998) can also impact this NAO-induced PEA in the subtropical gyre. In the
83 subpolar region, PEA come primarily from changes in local heat fluxes but also
84 from changes in the rates at which the water is imported and exported from the
85 interior basin.

86 As described above, the NAO is an essential driver of both immediate and
87 delayed oceanic variability (see also Lohmann et al 2009). However, recent work
88 of Hakkinen et al (2011a,b) suggests that one has to go beyond the sole NAO
89 contribution to understand the observed changes. In particular, the NAO fails
90 to explain the warming and salinization of the early 2000s in the North-Eastern

91 Atlantic. They argue that the latter could be due to the decadal fluctuations
92 of winter blocking conditions assessed in their study from the NOAA-20CR re-
93 analysis (Compo et al 2011) through traditional atmospheric metrics based on
94 daily variance of mean sea-level pressure (MSLP) anomalies. The blocking associ-
95 ated space-time structure of wind-anomalies, the so-called “gyre-mode” (Hakkinen
96 et al 2011a), is related to the second mode of variability in the North-Atlantic
97 atmospheric circulation, the so-called East-Atlantic Pattern (EAP, Barnston and
98 Livezey 1987). When EAP dominates atmospheric variability, the subtropical gyre
99 expands northward and the subpolar gyre shrinks; this facilitates the invasion of
100 warm, salty subtropical water into the eastern subpolar gyre.

101 The relative importance of NAO versus EAP atmospheric patterns in forc-
102 ing ocean circulation thus still appears to be an open question according to the
103 literature. The major goal of this study is to determine which large-scale atmo-
104 spheric circulation is responsible for the interannual SSH variability in the North
105 Atlantic subtropical gyre estimated from satellite and tide-gauge data. The atmo-
106 spheric anomalous circulation is assessed here through the weather regime (WR)
107 circulation paradigm, preferred to classical modes of variability. WRs have been
108 thoroughly studied in the literature (Vautard 1990; Michelangi et al 1995, among
109 others) and shown to be very efficient at capturing the interannual variability of
110 the surface ocean forcing in the North Atlantic (Cassou et al 2011). A second
111 objective is to clarify which mechanisms drive the ocean response to changes in
112 atmospheric conditions described by the WRs. The paper is organized as follows.
113 Section 2 describes the data and the methodology used in this study. Section 3 de-
114 scribes the observed winter North Atlantic WR ; a comparison between EOF and
115 WR circulation patterns is provided. Section 4 depicts the relationship between

116 WR occurrences and observed subtropical SSH anomalies. Section 5, based on a
117 simple linear planetary geostrophic model, investigates the physical mechanism at
118 work. Conclusions are given in section 6.

119 **2 Data and methodology**

120 **2.1 Subtropical sea-level**

121 Subtropical sea-level anomalies are extracted from two different datasets. We first
122 use AVISO Maps of Absolute Dynamic Topography (MADT, Ducet et al 2000),
123 available from October, 1992 to March, 2010. MADT maps are first regrided at a
124 coarser resolution (1° , similarly to Cabanes et al 2006). As winter weather regimes
125 occurrences are determined over winter, yearly averaged MADT anomalies are
126 computed from December to Novembre in order to keep the continuity of winter
127 months. As the dataset is not complete in 1992 and 2010, those years are discarded.
128 Additionally, a subtropical MADT time-series is computed by the averaging of
129 MADT anomalies over the box (64°W - 73°W , 24°N - 30°N), which encompasses
130 the subtropical gyre core without being influenced by the Gulf-Stream.

131 As the AVISO yearly time series spans a very short time-period (17 years), it is
132 completed by a longer record. We use tide-gauge data at Bermuda, located in the
133 subtropical gyre. Data were obtained from the Permanent Service for Mean Sea
134 Level (PSMSL, <http://www.psmsl.org/>), station Esso Pier/St Georges (32.367°N ,
135 64.700°W), between the period 1949 – 1998. To recover the missing values in the
136 PSMSL annual time series, due to some missing data in the monthly records,
137 we proceed as follows. The inverted barometer correction, following Ponte (2006),
138 is first applied to non-missing data of the raw PSMSL monthly time-series. A

139 linear trend of 1.2 mm/year , which is comparable with the existing literature
140 (e.g. Bindoff et al 2007), is removed from this monthly time series and anomalies
141 are calculated by subtracting the mean seasonal cycle. Values are finally yearly
142 averaged according to the same December-November average convention. We verify
143 that our yearly index, which spans 50 years, is correlated at 0.98 to the one given
144 by PSMSL (not shown).

145 2.2 Classification into weather regimes

146 The WR framework, based on daily circulation changes, accounts for the exis-
147 tence of preferred large-scale spatial states of the extratropical atmosphere set by
148 the stationary waves (Molteni et al 1990). The WR framework differs from fixed
149 station indices such as the traditional NAO index (Hurrell 1995), polluted by circu-
150 lations that are unrelated to the latitudinal alternation of the mean westerly flow
151 which defines the NAO itself (e.g Hurrell and VanLoon 1997). It also differs from
152 the traditional decomposition in modes of variability based for instance on EOF
153 or Singular Value Decomposition that makes symmetry assumptions for spatial
154 fluctuations. Additionally, the WR paradigm also accounts for time-scale inter-
155 action: weather changes are interpreted as transitions between WR while climate
156 variability is understood in terms of time-integration of daily WR occurrences and
157 internal characteristics (strength for instance) over the time-scale of interest. This
158 temporal integration property is promising for ocean variability studies (Minvielle
159 et al 2011), the ocean being often viewed as the integrator of atmospheric noise
160 (Frankignoul et al 1997).

161 To decompose atmospheric variability into WRs, we proceed as follows. NCEP-
162 NCAR (Kalnay et al 1996) daily maps of mean sea-level pressure (MSLP) anoma-
163 lies are computed inside the North-Atlantic domain (20°N - 80°N , 80°W - 30°E) by
164 removing a smoothed seasonal cycle (two harmonics retained). Winter (December-
165 January-February-March, hereafter DJFM) days are selected and MSLP anomalies
166 are normalized by the cosine of the latitude. The classification is done in EOF space
167 in order to reduce the degrees of freedom and thus facilitate the calculation. 20
168 EOFs that explain 98.9% of the total variance are retained. It should be noted
169 that contrary to Ayrault et al (1995) or Smyth et al (1999), no filtering is applied
170 to our data. This allows us to keep the synoptic-scale variability (2 – 6 days), the
171 slow-synoptic processes (6 – 11 days) and the low frequency variability (11 – 30
172 days) described in Gulev et al (2002). Part of the ultra-high frequency variability
173 (UHFV, 6h to 2 days) is lost by the daily averaging. Even if the variance associated
174 with UHFV is small, associated small scale events can lead to significant winds,
175 which will thus not be considered here.

While there are many classification techniques (mixture model clustering: Smyth et al 1999; non-linear equilibration: Vautard and Legras 1988, Vautard 1990), we use the k -mean algorithm described in Michelangi et al (1995) and Cassou (2008), which relies on the recurrence property of the weather regimes. The aim of the method is to agglomerate days that share some resemblance (Euclidian criteria). It assumes that the number of clusters, k , is known. The algorithm, described in Michelangi et al (1995), is as follows. k days are randomly chosen among all the dataset and their anomalous circulations define the k centroids C_k (initial seeds). Then, the method attributes to each day x the cluster that minimizes the Euclidian distance between x and C_k , that we call $d(x, C_k)$. This initial partition,

that we call P_k^0 , is used to re-compute the centroids by averaging all the days that belong to the same regime. We call these new centroids C_k^0 . The aggregation is iteratively repeated until the sum of variances within clusters of the n^{th} iteration, defined as:

$$W(P^n) = \sum_{k=1}^N \sum_{x \in C_k^n} d^2(x, C_k^n) \quad (1)$$

reaches a local minimum. As this method strongly depends on the initialization of the algorithm, the entire process is repeated 50 times for as many partitions. The one that minimizes the ratio of the sum of variances within clusters, $W(P)$, on the sum of variances outside clusters, $J(P)$, defined as:

$$J(P) = \sum_{k=1}^N \sum_{x \notin C_k} d^2(x, C_k) \quad (2)$$

176 is selected. Finally, daily occurrences are summed over DJFM days from 1949 to
177 2010 to obtain a time-series of yearly occurrences for each regime.

178 One limitation of the k -mean algorithm is the assumption that the number
179 of regimes is a priori known. However, Michelangi et al (1995) determined that
180 the number of clusters that allows classificability and reproducibility is 4, which
181 is the value determined from other methods (Vautard 1990). In the following, we
182 thus retain 4 winter weather regimes. A second limit, as mentioned in Smyth et al
183 (1999), is that this algorithm is inadequate if there is strong overlapping in the spa-
184 tial patterns of the regimes. Finally, most studies that deal with weather regimes
185 use geopotential height to compute weather regimes (Vautard 1990; Michelangi
186 et al 1995; Smyth et al 1999; Cassou et al 2011). We preferred to use MSLP, sim-
187 ilarly with Santos et al (2005), as MSLP can easily be related to surface winds.
188 We checked that comparable centroids and yearly occurrences are obtained using
189 anomalies of geopotential height at 500 hPa (not shown).

190 3 North-Atlantic weather regimes

191 The four winter weather regimes that we obtain are depicted in figure 1 (left
192 panels): the Atlantic Ridge (AR) characterized by an anticyclonic anomaly off
193 Europe, the Scandinavian-Blocking (BLK) dominated by a meridional pressure
194 dipole, north of 40°N , with an anticyclonic anomaly over northern Europe and a
195 cyclonic circulation between Greenland and Iceland, and the Greenland Anticy-
196 clone and Zonal regimes linked to the negative and positive phases of the NAO,
197 respectively. NAO- is characterized by a positive anomaly north of 50°N centered
198 around Greenland and aligned at 30°W with a negative pressure anomaly south of
199 50°N . NAO+ is dominated by negative anomalies between Iceland and the North
200 Sea while positive anomalies prevail south of 50°N . As shown in figure 1 (right
201 panels, blue bars), winter occurrences time series highlight a strong interannual to
202 decadal variability with neither pronounced nor significant trends.

203 Weather regimes have been shown to impact the “storm track” position. Ayrault
204 et al (1995) used the 2 – 6 days variance of geopotential height at 500 *hPa* (Z_{500})
205 as a proxy for the eastern position of the jet. The author states that NAO+ and
206 NAO- are more likely to affect northern and southern Europe, respectively, while
207 blocking regimes are likely to impact North-Eastern America. Rudeva and Gulev
208 (2011), using clustering techniques on cyclone observations, suggest that cyclones
209 formed in the Gulf-Stream region under NAO+/NAO- conditions are likely to end-
210 up in the Northeastern/Eastern Central Atlantic, respectively. On the other hand,
211 cyclones generated under AR conditions will decay in the Labrador-Sea while cy-
212 clones formed under blocking regimes will decay in the Southeastern Atlantic. We
213 performed a similar diagnosis as Ayrault et al (1995) to determine the position of

214 the eastern part of the jet within our four regimes. We use NCEP/NCAR (Kalnay
215 et al 1996) 2–6 days Z_{500} anomalies and computed the standard deviation within
216 each cluster (figure 2, color shading) and compare it with the climatological one
217 (figure 2, black contours). For AR, one can see that the climatological core of vari-
218 ability, localized off North-Eastern America, is tilted toward the Labrador-Sea,
219 consistently with Gulev et al (2002). There is also a core of high standard devia-
220 tion located in the Irminger Sea. In BLK, we notice that the variability is higher
221 in the North-Eastern America, while there seems to be a Northeastern tilt of the
222 Eastern part of the jet, probably due to the long-lasting anticyclone off Europe
223 (figure 1). The standard deviation in NAO- seems weaker and more zonal, while
224 in NAO+ it has a greater zonal extension. This seemingly implies more cyclones
225 in Northeastern Atlantic, consistent with Rudeva and Gulev (2011).

226 As described above, the WR paradigm differs from the traditional decomposi-
227 tion in modes of variability, which, by construction, makes symmetry assumptions.
228 Figure 1 (left panels) contrasts the MSLP patterns obtained from winter WR de-
229 composition (color shading) to those of the corresponding modes of variability.
230 The latter are obtained from EOF decomposition (black contours) performed on
231 DJFM averages of MSLP anomalies over the same North-Atlantic domain than
232 the WR. From figure 1, we can infer that AR is the positive phase of the EAP
233 (Barnston and Livezey 1987, 2nd EOF of MSLP) and BLK is the positive phase of
234 the so-called Scandinavian (SCAN) pattern (3rd EOF of MSLP). Finally, NAO-
235 and NAO+ project respectively on the positive and negative phases of the NAO
236 (1st EOF of MSLP). From figure 1, it is worth noticing that the spatial symmetry
237 assumption is not valid for the NAO. Indeed, the spatial pattern of NAO_{EOF} is
238 closer to NAO_{-WR} than to NAO_{+WR} obtained from classification: the NAO_{+WR}

239 northernmost negative anomaly is shifted eastward and the southernmost positive
240 anomaly is tilted south-eastward. Such a difference is associated with the intrinsic
241 dynamics of the upper-level tropospheric jet and is inherent to the two states of
242 its latitudinal position (Cassou et al 2004).

243 Consistently, the correlation between NAO_{EOF} index (figure 1, red line, defined
244 as the 1st normalized principal component of MSLP anomalies) and $NAO+WR$
245 occurrences is 0.67 while the correlation between NAO_{EOF} index and $NAO-WR$ oc-
246 currences is higher and reach -0.89 . Regarding AR_{WR} regime, there is a good cor-
247 respondence with the EAP_{EOF} pattern, although the maximum positive anomaly
248 is shifted North-Eastward in AR_{WR} compared to EAP_{EOF} ; as expected, the two
249 time-series are well correlated ($R=0.75$). The SCAN pattern is somehow differ-
250 ent from BLK and the two time series are less correlated. A possible cause for
251 this discrepancy is the orthogonality constraint of the EOF decomposition and
252 also the fact that “inverse blocking” events do not exist in nature as opposed to
253 $SCAN_{EOF}$ (by construction).

254 To summarize, the consideration of winter WR rather than the consideration
255 of classical EOF modes of variability allows to take into account the NAO spatial
256 asymmetry, the sole existence of blocking states without any constraint of orthog-
257 onality, which could lead to unrealistic spatial patterns. As a consequence, in the
258 following, the atmospheric variability in this study is only assessed through the
259 WR paradigm.

260 4 Subtropical sea-level response to weather regimes

261 The impact of wintertime WRs on sea-level anomalies can occur via mechanisms
262 of different nature. At seasonal and interannual timescales, the so-called inverted
263 barometer effect links SSH variations in ocean basins to the variation of surface
264 atmospheric pressure (Ponte 2006; Tsimplis and Shaw 2008; Woodworth et al 2010,
265 and references therein). This effect is not considered here as inverted barometer
266 corrections have been applied to the sea-level observations.

267 Weather regimes are associated with wind-anomalies (consistent with MSLP
268 patterns, figure 3, black arrows) and air-temperature anomalies (not shown), that
269 are traditionally assessed by daily composites. AR is dominated by a strong an-
270 ticyclonic anomaly off Europe and by a surface warming centered at the intergyre
271 region and extending in the north-western subpolar gyre. BLK depicts anticyclonic
272 anomalous circulation centered on Europe that prevents the mean Westerlies to
273 penetrate inland. Temperatures are colder off Newfoundland while warmer con-
274 ditions occur in the GIN seas due to the low-level advection of warm air from
275 the South. NAO- (resp. NAO+) is characterized by a reduction (resp. strength-
276 ening) and southward (northward) shift of the mean Westerlies and the Trade
277 winds in the subtropics that imprint a tripolar temperature pattern in latitude
278 (Cayan 1992), with a warming (resp. cooling) in the Labrador Sea/subtropics and
279 a cooling (resp. warming) in the GIN seas and the midlatitudes.

280 Those wind and air-temperature anomalies can lead to subtropical SSH re-
281 sponse via either halosteric/thermosteric effects or the dynamical adjustment to
282 the wind-stress forcing. The first mechanism corresponds to the thermal/haline di-
283 latation of the ocean water column induced by temperature changes (Tsimplis et al

284 2006) or changes in the global fresh water budget (e.g. icecaps melting, Stammer
 285 et al 2011). Those changes can be induced either by changes in heat/freshwater
 286 fluxes from the atmosphere to the ocean or by anomalous tracer advection. The
 287 second mechanism, associated with the long-term changes of open ocean wind
 288 stress curl, induces both a barotropic (Sverdrup-like dynamics) and a baroclinic
 289 (westward propagation of Rossby waves) ocean response (Sturges and Hong 1995;
 290 Sturges et al 1998; Ezer 1999; Hong et al 2000; Cabanes et al 2006). It is shown
 291 that such a mechanism can explain locally as much as 40% of the decadal variance
 292 in the Atlantic subtropical gyre (Cabanes et al 2006) and is likely to be the dom-
 293 inant one. Our working hypothesis will thus be that subtropical SSH response to
 294 WRs is driven by open ocean wind-stress curl.

295 As a first step to characterize the ocean response to winter WR wind circula-
 296 tions, we compute the corresponding Sverdrup transport anomaly composites $\widetilde{\psi}_{Sv}$
 297 (figure 3, color shading) as:

$$\widetilde{\psi}_{Sv}(x, y) = \frac{1}{\rho_0 \beta} \int_{x_E}^x \text{curl}_z(\widetilde{\tau}(x', y)) dx' \quad (3)$$

298 where $\rho_0 = 1030 \text{ kg m}^{-3}$ is the reference density of sea-water, β the meridional
 299 gradient of the Coriolis parameter, $\widetilde{\tau}$ the wind stress anomaly associated with
 300 WRs (figure 3, black arrows) and x_E the position of the Eastern boundary. These
 301 anomalies can be related to the mean pattern of the subpolar and subtropical gyre
 302 shown in figure 4.

303 AR is characterized by strong positive anomalies in the Labrador Sea associ-
 304 ated with anomalous southerly winds that contrast with slackened westerlies at
 305 midlatitudes (between 20° and 40°N). BLK anomalies are very weak, except for

306 a positive anomaly south of Iceland. NAO- is characterized by a positive anomaly
307 in the northern boundary of the Labrador Sea and Irminger Sea and at 30°N ,
308 and a negative anomaly between 40°N and 50°N in the intergyre region. NAO+
309 is characterized by opposite anomalies although shifted southward compared to
310 NAO- in agreement with the spatial asymmetry of the two NAO phases captured
311 through WR. For AR, note that the Sverdrup transport anomalies project very
312 well onto the mean position of the gyres (figure 4a); hence AR is expected to play
313 a central role in the subtropical gyre variability consistently with the (Hakkinen
314 et al 2011a) “gyre-mode” (their figure 3A).

315 To further estimate the possible roles of WR in forcing the North Atlantic
316 subtropical SSH variability, we calculate the correlations between WR winter oc-
317 currences and the annual subtropical SSH anomaly index (after removing a linear
318 trend). A correlation of -0.34 is obtained with AR yearly occurrences over 1993-
319 2009, significant at the 80% level (table 1). The confidence interval is computed by
320 a Student test, in which the degree of freedom is multiplied by a correction factor
321 depending on the 1 year-lag autocorrelation of each time series (Bretherton et al
322 1999, their equation 31). No correlations are found for neither NAO+ or NAO-
323 while a positive correlation of 0.36 is found with BLK.

324 As documented earlier, AR regime is characterized by a persistent anticyclonic
325 anomaly off Europe (figure 3) that displaces the climatological zero-wind-stress
326 curl northward (figure 4, left panel, red contours). Considering simple Sverdrup
327 balance, this causes a decrease of subtropical SSH as confirmed in figure 4 (right
328 panel) from MADT composites. The latter are computed for extreme AR years,
329 defined as winters for which the seasonal occurrences are greater than one standard
330 deviation. When AR winter events are frequent, a large scale negative anomaly

331 encompasses the subtropical gyre, consistently with the correlation previously dis-
332 cussed. The subpolar gyre is also characterized by positive anomalies that are
333 stronger in its eastern part and indicate a weakening of circulation there. All to-
334 gether, this is consistent with the anomalous Sverdrup contribution from WR wind
335 characteristics as discussed above.

336 The results presented so far suggest the importance of AR for subtropical SSH
337 interannual variability. However, those could be criticized because of the shortness
338 of the AVISO time series. In order to corroborate our findings, we have used the
339 observed data from tide-gauge at Bermuda (located in the subtropical gyre, figure
340 3, black point), to compute similar correlations, but over a much longer period of
341 time (50 years vs. 17 years for AVISO). Maximum correlation at -0.39 , significant
342 at the 95% level, is found again for AR (table 1) and consistently with AVISO, no
343 significant correlations are found for NAO+ and NAO-. The correlation for BLK
344 observed in the AVISO dataset no longer stands (0.17 , not significant at the 95%
345 level) and could therefore be attributed to the shortness of the data or to some
346 non stationarity of the ocean-atmosphere relationship yet to be investigated.

347 The correlations previously described simply give the information that sub-
348 tropical SSH and AR occurrences significantly covary in time over 1948-1998. No
349 information on the amplitude of the AR-induced SSH anomalies nor on the station-
350 arity of the relationship has been provided so far. The temporal evolution of the
351 AR-induced signal of Bermuda SSH is now reconstructed (figure 5, solid line) by
352 linearly regressing the normalized AR occurrences onto the SSH index. The regres-
353 sion coefficient estimated over 1948-1998 equals -17.5 mm per standard deviation
354 of winter AR occurrences. Light grey bars are the tide-gauge observations which
355 are used for the computation, dark grey bars from 1998 onwards are independent

356 data taken from the tide-gauge data but past the missing gap (see PSMSL web-
357 site). The latter can be used as cross-validation to assess the skill of the method.
358 The reconstructed signal does capture a large part of the decadal variability up to
359 the mid-70s in agreement with the strong dominance of AR over those decades.
360 While interannual fluctuations in the 80s and early 90s are reproduced to some
361 extent, the late 70s SSH significant rise is completely missed. A possible cause is
362 that the late 70s decade is characterized by strong NAO- events between 1977 and
363 1980 (figure 1) preceded by years of strong BLK. Both have a local imprint around
364 Bermuda (not shown) and may be lowering the impact of AR, that is less frequent
365 in that period. Note that the variance of the reconstructed time series is weaker
366 than the observed one as expected by construction using regression models (von
367 Storch 1999).

368 **5 Mechanisms of interannual subtropical SSH variability in response** 369 **to WR**

370 As stated earlier, we propose that subtropical SSH response to WRs is driven by
371 open ocean wind-stress curl. This working hypothesis discards the thermosteric/halosteric
372 effects caused by atmospheric heat/freshwater fluxes and by tracer advection. The
373 correlations discussed in the above seem to indicate that the AR anticyclonic circu-
374 lation, which tilts the wind-stress curl northward, causes a decrease in SSH yearly
375 anomalies.

376 In order to test our hypothesis, we have computed the wind-driven barotropic
377 η_p and baroclinic η_c components of sea-level from observed daily wind stress curl

378 following Cabanes et al (2006) linear planetary geostrophic model (their equations
379 11 and 20):

$$\eta_p(x, y, t) = \int_{x_e}^x \frac{f^2}{H\beta g} \text{curl} \left(\frac{\tau}{\rho_0 f} \right) \quad (4)$$

$$\eta_e(x, y, t) = -C_{rn}^{-1} \int_x^{x_e} \left[A_n \text{curl} \left(\frac{\tau}{\rho_0 f} \right) \right] (x', y, t - t_{x'}) dx' \quad (5)$$

380 where $t_{x'} = (x - x_{x'})/C_{rn}$ is the propagation time of the wave generated by local
381 atmospheric forcing east of longitude x , $C_{rn} = -\beta/\lambda_n^2$ is the wave propagation
382 speed of the n^{th} baroclinic mode (which eigenvalue is λ_n) and A_n the wind-stress
383 curl projection on this mode. The derivation of those two equations, described
384 in Cabanes et al (2006), relies on planetary geostrophic (PG) dynamics, neglects
385 bottom topography, advection by the mean currents and assumes a rigid lid. The
386 wind-stress forcing is implemented as a body force in the mixed layer of constant
387 depth (100 m). The values of C are computed by inversion of the eigenvalue prob-
388 lem:

$$\partial_z \left(\frac{f^2}{N^2} \partial_z F \right) + \lambda^2 F = 0 \quad (6)$$

389 where $F(z)$ is the vertical baroclinic structure, λ the corresponding eigenvalue
390 and N^2 the Brunt-Vaisala frequency (computed from *World Ocean Atlas 2005*
391 climatology Locarnini et al (2006); Antonov et al (2006) following the procedure
392 of Chelton et al (1998)). Equation 6 is verified by an infinity of orthogonal vertical
393 modes but, consistently with Cabanes et al (2006), the first baroclinic mode is
394 found to be dominant in the subtropical area. We consistently discard the higher-
395 ranked modes in our study. The values of C and A are longitude dependent but,

396 similarly to Cabanes et al (2006), we have used their zonal means. The computation
397 has been performed at $(33.3N, -78.8W)$, where C and A are equal to $-0.025 m.s^{-1}$
398 and 11.10^{-4} respectively. We have chosen daily wind fields instead of monthly
399 fields because the latter give too weak an amplitude of SSH (Cécile Cabanes,
400 personal communication) and also to better account for the intrinsic properties
401 and advantages of the WR as above-described. NCEP/NCAR daily wind fields
402 are available from 1948 to 2006. The first five years of the PG sea-level anomalies
403 were discarded as part of the spin-up.

404 Total (ie. barotropic+baroclinic) contribution of wind-stress curl to sea-level
405 anomalies is depicted in figure 5 (dashed line) and a significant correlation of 0.53
406 is found with observations (table 1). Note that the amplitude of the barotropic
407 component is approximately 3 times smaller than the baroclinic one (not shown).
408 This is consistent with the results of Hong et al (2000) who argue that, to first
409 order, Bermuda sea-level can be approximated by the first baroclinic mode. Inter-
410 estingly, when the regression (solid black line) has some skill to reproduce observed
411 SSH variability, so does the PG SSH anomalies. This tends to confirm that AR
412 impact on Bermuda SSH is very likely due to the strong anticyclone off Europe,
413 which tilts the zero wind-stress curl northward, and brings some confidence in our
414 physical interpretation of the observations. Especially, the dramatic drop of 1970
415 is well captured by the regression and the PG model. This is consistent with Ezer
416 (1999) who argues that the 1970 drop is due to changes in open-ocean wind-stress
417 curl. However, Ezer (1999) attributes it to changes in NAO while we say that it is
418 due to changes in AR regime.

419 So far, correlations have been computed using the occurrences of wintertime
420 WRs, considering the higher variance and mean values of the atmospheric forc-

421 ing with respect to the other seasons (Minvielle et al 2011). Using the planetary
422 geostrophic model, we will verify that summer atmospheric dynamics play indeed
423 a lesser role in the total interannual changes. We run two additional sensitivity
424 experiments in which the PG model is forced with DJFM daily wind-stress and
425 climatological values for the other months in the first one, and observed JJAS
426 daily winds, climatology for the rest of the year in the second one. Results shown
427 in figure 6 confirm that the variance of the interannual time-series is indeed mostly
428 due to DJFM winds. The sole exception where the two seasons contributions are
429 comparable is in the 1960s and the mid-2000s. The strong positive observed SSH
430 decadal anomalies at the early period can thus be interpreted as the integration
431 of yearly persistent high pressure anomalies over the North Atlantic basin that
432 projects on AR as diagnosed in Cassou et al (2011) from summertime weather
433 regime decomposition. Spring and Fall months (ie October-November and April-
434 May) are treated as intermediate months dominated by either summer and winter
435 dynamics (Minvielle et al 2011); they are therefore not considered here.

436 In the results above-described, we have used spatial uniform wave propagation
437 speed and wind-stress curl projection on the first baroclinic mode. We have run
438 additional sensitivity experiments in which C is set at the minimum or at the
439 maximum value at the Bermuda latitude. We found that changes in C have a non-
440 negligible impact on interannual variability given by the PG model. The time-series
441 are indeed time shifted by one year compared to the original one. Note that the
442 choice of the mean value ($-0.025 m.s^{-1}$) appears to be the best as it maximizes the
443 correlation between reconstructed series and observations (not shown). Changes
444 in A have no effect, as A appears in equation 5 as a multiplying factor.

6 Discussion and conclusion

Since atmospheric modes of variability have been described in the literature (e.g. Barnston and Livezey 1987), many studies investigated the ocean response to those modes of variability, focussing essentially on the impact of the NAO on the circulation and hydrography in the North Atlantic. However, recent studies highlighted the role of the East-Atlantic Pattern (EAP). Msadek and Frankignoul (2009) suggest that multidecadal variability of Atlantic Meridional Overturning Circulation (AMOC) is closely related to EAP, while Langehaug et al (2012) suggest that subpolar gyre strength is significantly correlated with the EAP. Hence the EAP is at least as important as the NAO in driving variability in the North Atlantic. Nevertheless, these three studies rely on the analysis of coupled climate models which have important biases in the convection sites.

The present study is a step toward the investigation of such a relationship in observations, with a special focus laid on subtropical gyre variability. The question we address is which large-scale atmospheric pattern influences subtropical gyre variability, and through which mechanism. We use the weather regime (WR) paradigm to describe the wintertime North Atlantic atmospheric variability and investigate its impact on subtropical SSH interannual-to-decadal variability. WR treated as populations of days sharing common large-scale atmospheric circulation anomalies are different from classical modes of variability estimated for instance through EOF because they have no orthogonality constraint and account for potential spatial asymmetries of the patterns. This is especially true for NAO+ and NAO- events and may be of central importance, as processes driving the variability of the mixed layer (turbulent and latent heat fluxes for example) are nonlinear

(Cassou et al 2011). WRs have been shown to be efficient in capturing surface forcing variability from daily-to-interannual timescale (Cassou et al 2011).

Over the longest time period of available record over Bermuda, we find that AR is the dominant atmospheric weather regime driving SSH variability in the subtropical gyre. Sverdrup transport anomalies related to AR conditions (windstress curl changes off Europe) show a positive anomaly north of 50°N and a negative anomaly south of it. The dipole projects very well on the mean position of the gyres and is thus very efficient in forcing the large-scale mean circulation. We considered tide-gauge data in the Bermuda available from 1948 to 1998 and only found a significant correlation between AR WR occurrences and Bermuda SSH. The sole barely significant relationship between SSH in Bermuda and the NAO could be obtained in the framework of our study when the period is restricted to 1958-1998. This suggests that the connection between the two, if any, is not stationary, or at least not overly dominant contrary to what has been suggested in previous studies. Over a limited period of time, independent satellite observations from 1993 onwards confirm that years with frequent AR conditions in winter lead to negative SSH anomalies that encompass the full subtropical gyre, Bermuda included, suggesting a weakening of subtropical gyre strength.

We used a simple planetary geostrophic model (PG) to explore the physical mechanisms linking wind-stress curl associated with daily wintertime WR and SSH interannual variability in Bermuda. The reconstructed signal using both the barotropic (Sverdrup like) and baroclinic (westward propagation of planetary waves) model components, which covary in phase, is highly correlated to observations suggesting that the largest part of the variability in Bermuda SSH is wind-driven. Sensitivity experiments confirm that most of the interannual signal is due

494 to winter wind conditions integrated over time while summer wind anomalies have
495 a second-order contribution to the yearly signal.

496 AR is closely related to the “gyre mode” defined in Hakkinen et al (2011a,b)
497 that is linked to the second EOF mode of wind-stress curl explaining part of
498 warm and saline intrusion from the subtropical gyre into the subpolar ocean. AR
499 also corresponds to the positive phase of the EAP and we verify that our results
500 are robust when using EAP time series instead of AR occurrences (correlation
501 of -0.34 between the EAP index and Bermuda SSH anomalies instead of -0.39
502 for AR). Consistently with Hakkinen et al (2011a,b) our finding highlights the
503 primarily importance of the atmospheric patterns of variability other than the
504 NAO to understand the North Atlantic ocean dynamics.

505 Our study mainly focused on the immediate (0-year lag) response of subtropical
506 SSH to changes in winter-weather regime occurrences. However, Curry and Mc-
507 Cartney (2001) suggest that remote mechanisms, such as Eighteen Degree Water
508 formation, Gulf-Stream inertial recirculation and deep-density structure, influ-
509 ence subtropical gyre variability. While remote (both in time and space) influence
510 of NAO on ocean circulation has been thoroughly studied (Eden and Willebrand
511 2001; Deshayes and Frankignoul 2008), our results demonstrate that the possible
512 influence of other modes of variability needs to be considered.

513 **Acknowledgements** NCEP Reanalysis data were provided by the NOAA/OAR/ESRL PSD,
514 Boulder, Colorado, USA, from their Web site (<http://www.esrl.noaa.gov/psd/>). The altimeter
515 products were produced by Ssalto/Duacs and distributed by Aviso, with support from Cnes
516 (<http://www.aviso.oceanobs.com/duacs/>). Tide gauge data were obtained from the Permanent
517 Service For Mean Sea Level website (<http://www.psmsl.org/>).

518 The authors acknowledge Cécile Cabanes for having provided us the matlab routines of
519 the baroclinic component of her model and for fruitful discussions.

520 Nicolas Barrier is supported by a PhD grant from Unniversité de Bretagne Occidentale,
521 Ifremer and Europôle Mer.

522 Anne-Marie Treguier, Christophe Cassou and Julie Deshayes acknowledge the CNRS.

523 **References**

524 Antonov J, Locarnini R, Boyer T, Mishonov A, Garcia H (2006) World Ocean Atlas 2005,
525 Volume 2: Salinity. NOAA Atlas NESDIS 62

526 Ayrault F, Lalaurette F, Joly A, Loo C (1995) North-Atlantic Ultra-High Frequency variability-
527 An introductory survey. *Tellus Series A-Dynamic Meteorology and Oceanography* 47(5,
528 Part 1):671–696

529 Barnston A, Livezey R (1987) Classification, seasonality and persistence of low-frequency at-
530 mospheric circulation patterns. *Monthly Weather Review* 115(6):1083–1126

531 Bindoff N, Willebrand J, Artale V, A C, Gregory J, Gulev S, Hanawa K, Qir CL, Levitus
532 S, Nojiri Y, Shum C, Talley L, Unnikrishnan A (2007) Observations: Oceanic Climate
533 Change and Sea Level. *Climate Change 2007: The Physical Science Basis Contribution*
534 of Working Group I to the Fourth Assessment Report of the Intergovernmental Panel on
535 Climate Change

536 Bretherton C, Widmann M, Dymnikov V, Wallace J, Blade I (1999) The effective number of
537 spatial degrees of freedom of a time-varying field. *Journal of Climate* 12(7):1990–2009

538 Cabanes C, Huck T, De Verdiere AC (2006) Contributions of wind forcing and surface heating
539 to interannual sea level variations in the Atlantic Ocean. *Journal of Physical Oceanography*
540 36(9):1739–1750

541 Cassou C (2008) Intraseasonal interaction between the Madden-Julian Oscillation and the
542 North Atlantic Oscillation. *Nature* 455(7212):523–527

543 Cassou C, Terray L, Hurrell J, Deser C (2004) North Atlantic winter climate regimes: Spatial
544 asymmetry, stationarity with time, and oceanic forcing. *Journal of Climate* 17(5):1055–
545 1068

-
- 546 Cassou C, Minvielle M, Terray L, Perigaud C (2011) A statistical-dynamical scheme for re-
547 constructing ocean forcing in the Atlantic. Part I: weather regimes as predictors for ocean
548 surface variables. *Climate Dynamics* 36(1-2):19–39
- 549 Cayan D (1992) Latent and sensible heat-fluxes anomalies over the Northern Oceans - Driving
550 the Sea-Surface Temperature. *Journal of Climate* 5(4):354–369
- 551 Chelton D, DeSzoeke R, Schlax M, El Naggar K, Siwertz N (1998) Geographical variability
552 of the first baroclinic Rossby radius of deformation. *Journal of Physical Oceanography*
553 28(3):433–460
- 554 Compo GP, Whitaker JS, Sardeshmukh PD, Matsui N, Allan RJ, Yin X, Gleason BE Jr, Vose
555 RS, Rutledge G, Bessemoulin P, Broennimann S, Brunet M, Crouthamel RI, Grant AN,
556 Groisman PY, Jones PD, Kruk MC, Kruger AC, Marshall GJ, Maugeri M, Mok HY, Nordli
557 O, Ross TF, Trigo RM, Wang XL, Woodruff SD, Worley SJ (2011) The Twentieth Century
558 Reanalysis Project. *Quarterly Journal of the Royal Meteorological Society* 137(654, Part
559 a):1–28
- 560 Curry R, McCartney M (2001) Ocean gyre circulation changes associated with the North
561 Atlantic Oscillation. *Journal of Physical Oceanography* 31(12):3374–3400
- 562 Curry R, McCartney M, Joyce T (1998) Oceanic transport of subpolar climate signals to
563 mid-depth subtropical waters. *Nature* 391(6667):575–577
- 564 Deshayes J, Frankignoul C (2008) Simulated variability of the circulation in the North Atlantic
565 from 1953 to 2003. *Journal of Climate* 21(19):4919–4933
- 566 Ducet N, Le Traon P, Reverdin G (2000) Global high-resolution mapping of ocean circula-
567 tion from TOPEX/Poseidon and ERS-1 and-2. *Journal of Geophysical Research-Oceans*
568 105(C8):19,477–19,498
- 569 Eden C, Willebrand J (2001) Mechanism of interannual to decadal variability of the North
570 Atlantic circulation. *Journal of Climate* 14(10):2266–2280
- 571 Esselborn S, Eden C (2001) Sea surface height changes in the North Atlantic Ocean related to
572 the North Atlantic Oscillation. *Geophysical Research Letters* 28(18):3473–3476
- 573 Ezer T (1999) Decadal variabilities of the upper layers of the subtropical North Atlantic: An
574 ocean model study. *Journal of Physical Oceanography* 29(12):3111–3124

-
- 575 Frankignoul C, Muller P, Zorita E (1997) A simple model of the decadal response of the ocean
576 to stochastic wind forcing. *Journal of Physical Oceanography* 27(8):1533–1546
- 577 Gulev S, Jung T, Ruprecht E (2002) Climatology and interannual variability in the intensity
578 of synoptic-scale processes in the North Atlantic from the NCEP-NCAR reanalysis data.
579 *Journal of Climate* 15(8):809–828
- 580 Gulev S, Barnier B, Knochel H, Molines J, Cottet M (2003) Water mass transformation in the
581 North Atlantic and its impact on the meridional circulation: Insights from an ocean model
582 forced by NCEP-NCAR reanalysis surface fluxes. *Journal of Climate* 16(19):3085–3110
- 583 Hakkinen S (1999) Variability of the simulated meridional heat transport in the North Atlantic
584 for the period 1951-1993. *Journal of Geophysical Research-Oceans* 104(C5):10,991–11,007
- 585 Hakkinen S, Rhines PB, Worthen DL (2011a) Atmospheric Blocking and Atlantic Multidecadal
586 Ocean Variability. *Science* 334(6056):655–659
- 587 Hakkinen S, Rhines PB, Worthen DL (2011b) Warm and saline events embedded in the merid-
588 ional circulation of the northern North Atlantic. *Journal of Geophysical Research* 116
- 589 Hong B, Sturges W, Clarke A (2000) Sea level on the US East Coast: Decadal variability caused
590 by open ocean wind-curl forcing. *Journal of Physical Oceanography* 30(8):2088–2098
- 591 Hurrell J (1995) Decadal Trends in the North-Atlantic Oscillation - Regional temperatures
592 and precipitations. *Science* 269(5224):676–679
- 593 Hurrell J, VanLoon H (1997) Decadal variations in climate associated with the north Atlantic
594 oscillation. *Climatic Change* 36(3-4):301–326
- 595 Joyce T, Deser C, Spall M (2000) The relation between decadal variability of subtropical mode
596 water and the North Atlantic Oscillation. *Journal of Climate* 13(14):2550–2569
- 597 Kalnay E, Kanamitsu M, Kistler R, Collins W, Deaven D, Gandin L, Iredell M, Saha S, White
598 G, Woollen J, Zhu Y, Chelliah M, Ebisuzaki W, Higgins W, Janowiak J, Mo K, Ropelewski
599 C, Wang J, Leetmaa A, Reynolds R, Jenne R, Joseph D (1996) The NCEP/NCAR 40-year
600 reanalysis project. *Bulletin of the American Meteorological Society* 77(3):437–471
- 601 Langehaug HR, Medhaug I, Eldevik T, Ottera OH (2012) Arctic/Atlantic Exchanges via the
602 Subpolar Gyre. *Journal of Climate* 25(7):2421–2439
- 603 Locarnini R, Mishonov J, Antonov, Boyer T, Garcia H (2006) *World Ocean Atlas 2005*,
604 Volume 1: Temperature. NOAA Atlas NESDIS 61

-
- 605 Lohmann K, Drange H, Bentsen M (2009) Response of the North Atlantic subpolar gyre to
606 persistent North Atlantic oscillation like forcing. *Climate Dynamics* 32(2-3):273–285
- 607 Michelangi P, Vautard R, Legras B (1995) Weather Regimes - Recurrence and quasi-
608 stationarity. *Journal of Atmospheric Sciences* 52(8):1237–1256
- 609 Minvielle M, Cassou C, Bourdalle-Badie R, Terray L, Najac J (2011) A statistical-dynamical
610 scheme for reconstructing ocean forcing in the Atlantic. Part II: methodology, validation
611 and application to high-resolution ocean models. *Climate Dynamics* 36(3-4):401–417
- 612 Molteni F, Tibaldi S, Palmer T (1990) Regimes in the wintertime circulation over northern
613 extratropics .1. Observational Evidence. *Quarterly Journal of the Royal Meteorological*
614 *Society* 116(491, Part a):31–67
- 615 Msadek R, Frankignoul C (2009) Atlantic multidecadal oceanic variability and its influence on
616 the atmosphere in a climate model. *Climate Dynamics* 33(1):45–62
- 617 Ponte R (2006) Low-frequency sea level variability and the inverted barometer effect. *Journal*
618 *of Atmospheric and Oceanic Technology* 23(4):619–629
- 619 Rudeva I, Gulev SK (2011) Composite Analysis of North Atlantic Extratropical Cyclones in
620 NCEP-NCAR Reanalysis Data. *Monthly Weather Review* 139(5):1419–1446
- 621 Santos J, Corte-Real J, Leite S (2005) Weather regimes and their connection to the winter
622 rainfall in Portugal. *International Journal of Climatology* 25(1):33–50
- 623 Smyth P, Ide K, Ghil M (1999) Multiple regimes in Northern Hemisphere height fields via
624 mixture model clustering. *Journal of the Atmospheric Sciences* 56(21):3704–3723
- 625 Stammer D, Agarwal N, Herrmann P, Koehl A, Mechoso CR (2011) Response of a Cou-
626 pled Ocean-Atmosphere Model to Greenland Ice Melting. *Surveys in Geophysics* 32(4-5,
627 SI):621–642
- 628 von Storch H (1999) On the use of “inflation” in statistical downscaling. *Journal of Climate*
629 12(12):3505–3506
- 630 Sturges W, Hong B (1995) Wind forcing of the Atlantic Thermocline along 32 degrees N at
631 low frequencies. *Journal of Physical Oceanography* 25(7):1706–1715
- 632 Sturges W, Hong B, Clarke A (1998) Decadal wind forcing of the North Atlantic subtropical
633 gyre. *Journal of Physical Oceanography* 28(4):659–668

- 634 Tsimplis M, Shaw A, Flather R, Woolf D (2006) The influence of the North Atlantic Oscillation
635 on the sea-level around the northern European coasts reconsidered: the thermosteric effects.
636 Philosophical Transactions of the Royal Society A-Mathematical Physical and Engineering
637 Sciences 364(1841):845–856
- 638 Tsimplis MN, Shaw AGP (2008) The forcing of mean sea level variability around Europe.
639 Global and Planetary Change 63(2-3, SI):196–202
- 640 Vautard R (1990) Multiple weather regimes over the North-Atlantic. Analysis of precursors
641 and successors. Monthly Weather Review 118(10):2056–2081
- 642 Vautard R, Legras B (1988) On the source of midlatitude low-frequency variability. Part 2: Non-
643 linear equilibration of Weather Regimes. Journal of Atmospheric Sciences 45(20):2845–
644 2867
- 645 Woodworth P, Pouvreau N, Woepplmann G (2010) The gyre-scale circulation of the North
646 Atlantic and sea level at Brest. Ocean Science 6(1):185–190

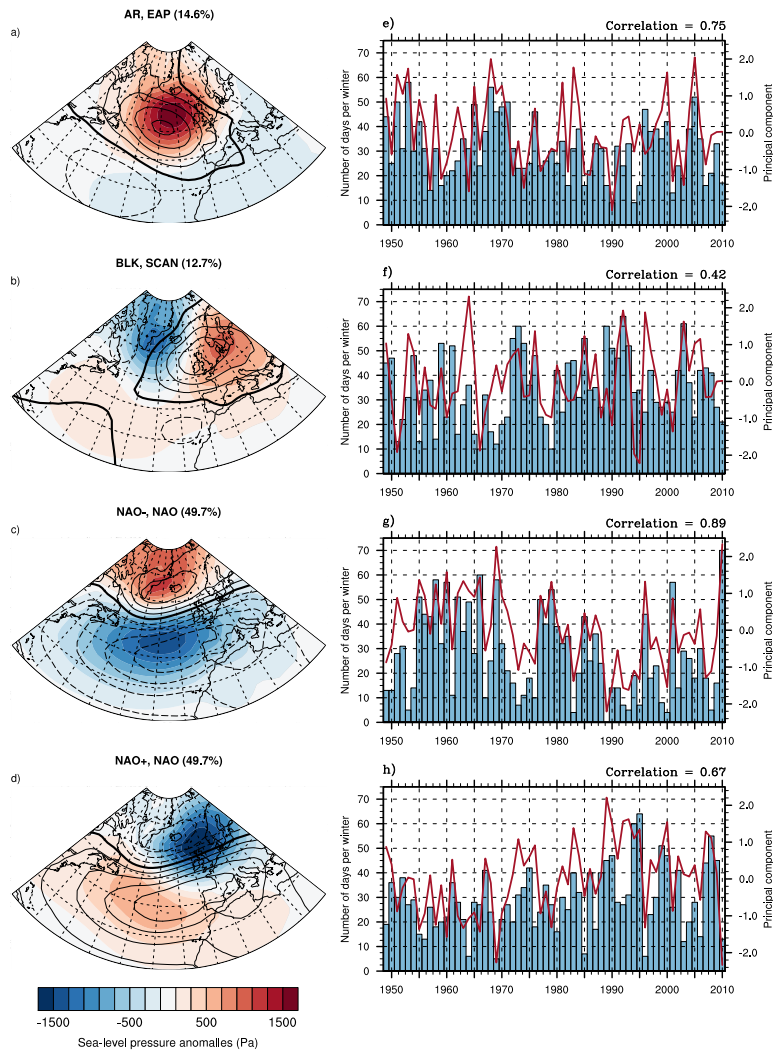


Fig. 1: (left) Centroids of daily sea-level pressure anomalies for the four weather regimes (colors, contour interval: 200 Pa) and EOF-derived modes of variability computed from DJFM averaged sea-level pressure anomalies (black contours, contour interval: 50 Pa). The variance explained by each EOF is indicated between parenthesis. (right) Number of days per winter of WR winter occurrences (bars) and corresponding principal components (PC) from EOF (see text for details). The correlations between the occurrences and the PCs are indicated. For panel c), the NAO_{EOF} pattern and associated PC are multiplied by -1 so that they share the same sign as the NAO- regime.

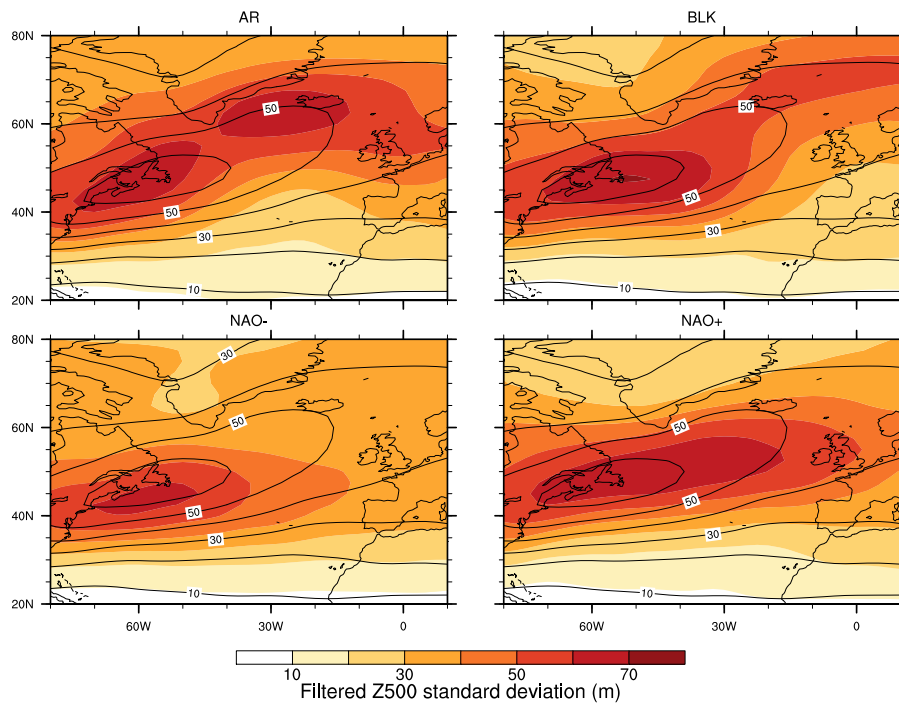


Fig. 2: Daily DJFM standard deviation of filtered (2 – 6 days) Z_{500} anomalies
(black contours: climatological, color shading: within each weather regime)

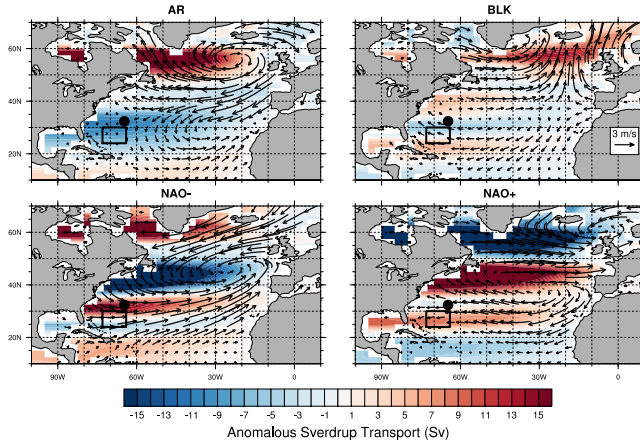


Fig. 3: Daily composites of winter wind-field anomalies (arrows, reference = 3 m.s^{-1}) and corresponding anomalous Sverdrup transport (colors, contour interval = 1 Sv). The black point shows the location of the Esso-Pier (Bermuda) station and the black rectangle our subtropical box used in the correlation (see text and table 1).

Table 1: List of correlations cited in the text. "AR-induced SSH" refers to the regressed reconstructed series (solid line in fig 5) and "PG model" refers to the linear solution calculated from daily wind fields (dashed line in figure 5 and black line in figure 6).

Time series			Period	Confidence interval	Correlation
AR winter occurrences	vs	Subtropical AVISO MADT	1993 – 2009	80%	-0.34
AR winter occurrences	vs	Observed Bermuda SSH	1949 – 1998	95%	-0.39
AR-induced SSH	vs	Observed Bermuda SSH	1949 – 1998	95%	0.39
PG model	vs	Observed Bermuda SSH	1954 – 1998	95%	0.53
AR winter occurrences	vs	PG model	1954 – 2006	95%	-0.53

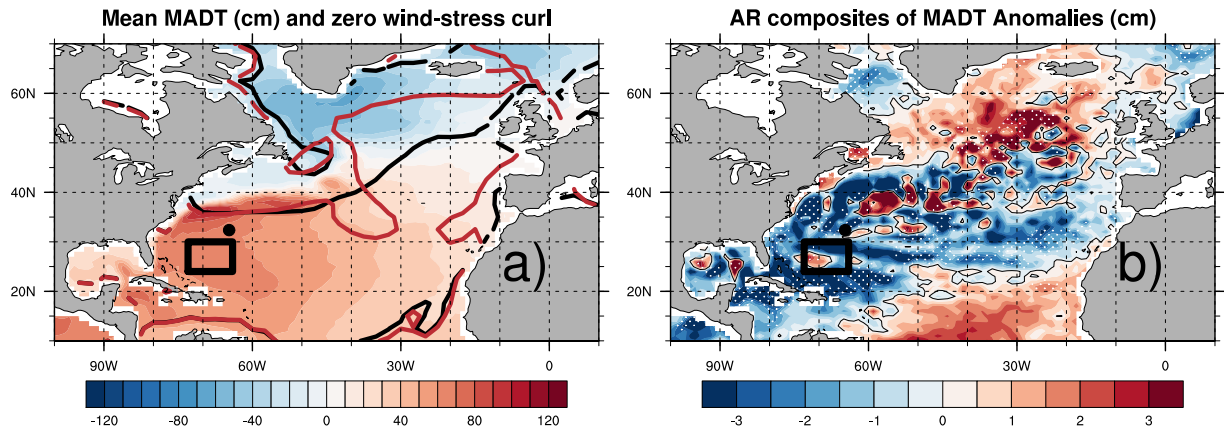


Fig. 4: (Left) Mean Map of Absolute Dynamic Topography (colors). Climatological (black contours) and AR composite (red contours) zero wind-stress curl. (Right) panel: Map of Absolute Dynamic Topography (MADT) anomalies composite for extreme Atlantic Ridge events (zero contours are depicted in black). Significant values, based on t-statistics at the 80% level of confidence, are white dotted.

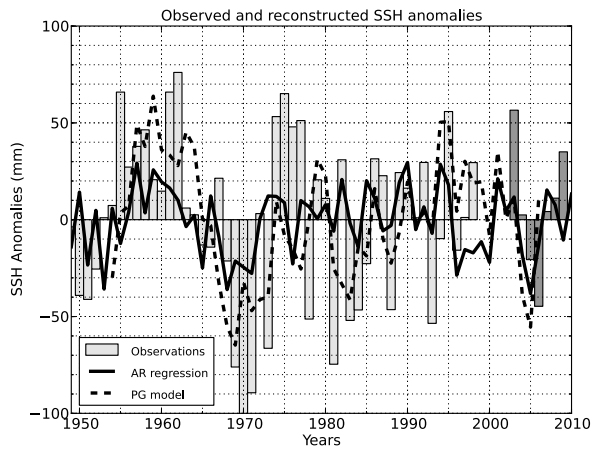


Fig. 5: Observed time-series of Bermuda Sea-Surface Height anomalies (in mm, light grey bars are the tide-gauge observations used in the regression while dark gray bars are independent tide-gauge observations), regressed SSH onto AR occurrences (solid line) and the planetary geostrophic model of sea-level (dashed line).

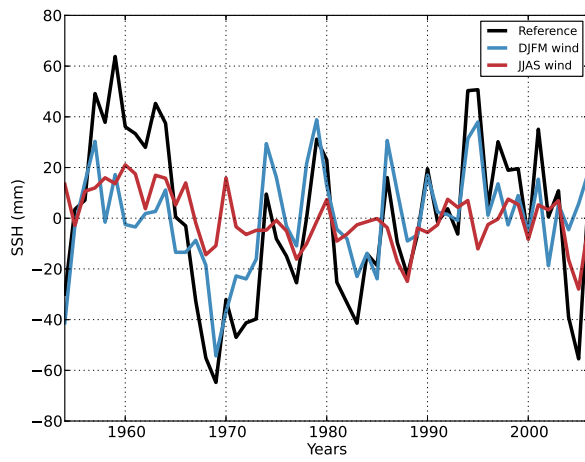


Fig. 6: Planetary geostrophic model forced by observed wind (black) and sensitivity experiments with variable DJFM wind only (blue) and variable JJAS wind only (red)